Research article

Determining acute ischemic stroke onset time using machine learning and radiomics features of infarct lesions and whole brain

Jiaxi Lu[1,2], Yingwei Guo[2,3], Mingming Wang[4], Yu Luo[4,*], Xueqiang Zeng[1,2], Xiaoqiang Miao[2,3], Asim Zaman[1,2], Huihui Yang[1,2], Anbo Cao[1,2] and Yan Kang[2,3,5,*]

[1] School of Applied Technology, Shenzhen University, Shenzhen 518060, China
[2] College of Health Science and Environmental Engineering, Shenzhen Technology University, Shenzhen 518118, China
[3] College of Medicine and Biological Information Engineering, Northeastern University, Shenyang 110169, China
[4] Department of Radiology, Shanghai Fourth People's Hospital Affiliated to Tongji University School of Medicine, Shanghai 200434, China
[5] Engineering Research Centre of Medical Imaging and Intelligent Analysis, Ministry of Education, Shenyang 110169, China

* **Correspondence:** Email: duolan@hotmail.com, kangyan@sztu.edu.cn.

Abstract: Accurate determination of the onset time in acute ischemic stroke (AIS) patients helps to formulate more beneficial treatment plans and plays a vital role in the recovery of patients. Considering that the whole brain may contain some critical information, we combined the Radiomics features of infarct lesions and whole brain to improve the prediction accuracy. First, the radiomics features of infarct lesions and whole brain were separately calculated using apparent diffusion coefficient (ADC), diffusion-weighted imaging (DWI) and fluid-attenuated inversion recovery (FLAIR) sequences of AIS patients with clear onset time. Then, the least absolute shrinkage and selection operator (Lasso) was used to select features. Four experimental groups were generated according to combination strategies: Features in infarct lesions (IL), features in whole brain (WB), direct combination of them (IW) and Lasso selection again after direct combination (IWS), which were used to evaluate the predictive performance. The results of ten-fold cross-validation showed that IWS achieved the best AUC of 0.904, which improved by 13.5% compared with IL (0.769), by 18.7% compared with WB (0.717) and 4.2% compared with IW (0.862). In conclusion, combining infarct lesions and whole brain features from multiple sequences can further improve the accuracy of AIS onset time.

Keywords: acute ischemic stroke; onset time; whole brain; machine learning; radiomics

1. Introduction

Stroke is a disease with high incidence, disability rate, mortality rate and recurrence rate and it has become one of the leading causes of death and disability worldwide [1]. Acute ischemic stroke (AIS) is caused by obstruction of blood flow in cerebral arteries, leading to downstream cerebral tissue hypoxia and local brain tissue damage and necrosis [2]. The treatment of AIS requires prompt restoration of cerebral blood flow through intravenous thrombolysis or endovascular thrombectomy in the early stages of symptom onset, and the selection of treatment method and success rate are closely related to the onset time [3].

Recombinant tissue plasminogen activator (rt-PA) is currently the preferred medication for treating AIS [3,4], which has been proven to reduce the thrombotic burden and long-term disability in patients [5], and it has become a part of the standard treatment protocol in stroke management guidelines across the globe. However, thrombolytic therapy has a strict time usage guideline, which can help patients quickly open blood vessels and restore cerebral blood supply within the time window [6], thereby reversing ischemic and hypoxic tissue to normal tissue transformation rather than continuing deterioration. In contrast, when the onset time exceeds the time window, it is difficult to restore brain cell function even with thrombolytic therapy, which may cause reperfusion injury and increase the risk of cerebral hemorrhage [7]. Additionally, determining the exact onset time in patients is often complicated by various factors, including delayed hospital admission, wake-up stroke, etc. [8,9]. Some studies have shown that 25–30% of AIS patients are excluded from intravenous thrombolysis treatment due to the inability to determine the exact onset time [10,11]. However, the onset of these patients may fall within the time window. Therefore, finding a way to determine the onset time accurately is necessary.

For patients with an unclear onset time, some studies suggest using diffusion-weighted imaging (DWI) and fluid-attenuated inversion recovery (FLAIR) mismatch to determine the "tissue clock" for assessing eligibility for intravenous thrombolysis [12,13]. However, this method can sometimes be overly rigorous in determining the onset time, potentially excluding patients who could have benefited from thrombolytic therapy due to their imaging characteristics [14]. Additionally, the use of imaging for "tissue clock" determination may also be influenced by subjective physician judgment. With the development of radiomics and artificial intelligence, image features have been widely used in stroke diagnosis and prognosis [15]. Several studies have developed various ML models based on imaging features derived from stroke images, providing evidence of ML algorithms' feasibility in determining the onset time and guiding rt-PA usage eligibility. Ho et al. [16] extracted lesion features from MR images, perfusion parameter maps and deep autoencoder feature maps, using ML models to classify the onset time. The best classifier achieved an area under the curve (AUC) of 0.765. Lee et al. [17] classified the onset time based on the radiomics features of the lesions from DWI and FLAIR sequences. The best classifier achieved an AUC of 0.851. Zhu et al. [18] segmented DWI and FLAIR's ROI based on deep learning and generated features, which were further inputted into five classification models and obtained robust accuracy through voting. Zhang et al. [19] developed a deep learning model for classifying the onset time based on the lesion's DWI and apparent diffusion coefficient (ADC) radiomics features, with an AUC of 0.754. As seen above, previous studies have focused on determining the onset time through quantitative analysis of information within the lesions,

often overlooking the information available from the whole brain. However, stroke occurrences can trigger responses throughout the whole brain. Therefore, it is necessary to investigate the relationship between whole brain radiomics features and stroke onset time.

To address these issues, we compared the predictive performance of different models based on lesions radiomics features and whole brain radiomics features and proposed a feature fusion strategy for comprehensive analysis of infarct lesions and whole brain information to improve the accuracy of classifying the onset time.

2. Materials and methods

2.1. Materials

We collected 537 AIS patients treated in the neurology department of the Shanghai Fourth People's Hospital, affiliated with the Tongji University School of Medicine, China, from January 2013 to September 2019.

A total of 72 patients were included in this study after the screening, and the inclusion and exclusion criteria were as follows (Figure 1): (1) The MR examinations were conducted within 24 hours of symptom onset; (2) Complete MR imaging sequences (ADC, DWI and FLAIR); (3) The actual treatment and National Institute of Health stroke scale (NIHSS) scores; (4) Occlusions of the middle cerebral artery (M1 segment); (5) Actual recorded stroke onset time. The onset time was classified into two classes based on the patients' actual recorded time of onset: Positive ($\leqslant 4.5$ h) and negative (> 4.5 h).
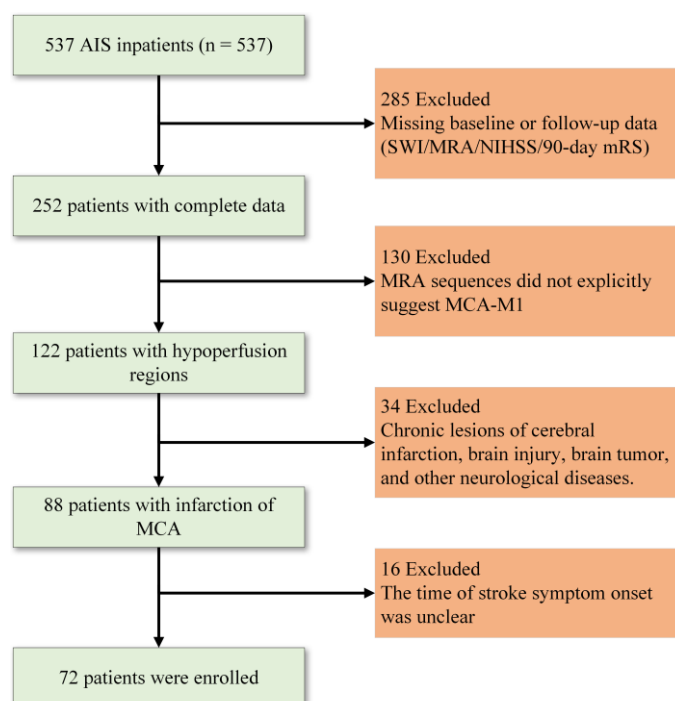

Figure 1. Flowchart of patient inclusion and exclusion criteria. SWI: susceptibility weighted imaging; MRA: magnetic resonance angiography; mRS: modified rankin scale; MCA: middle cerebral artery.

All MR images were scanned on a 1.5-Tesla MR scanner (Siemens, Munich, Germany). The parameters of DWI: b = 1000 s/mm^2; field of view, 230 × 230 mm^2; matrix size, 192 × 192; slices, 18; slice thickness, 5 mm; pixel spacing, 1.198 × 1.198 mm^2; repetition time, 3600 ms; echo time, 102 ms; bandwidth, 964 Hz/pixel; and EPI factor: 192. FLAIR: field of view, 201× 230 mm^2; matrix size, 448 × 512; slices, 20; slice thickness, 5 mm; pixel spacing, 0.449 × 0.449 mm^2; repetition time, 4000 ms; echo time, 92 ms; bandwidth, 190 Hz/pixel. Table 1 shows the details of patient information.

Table 1. Ischemic stroke patient cohort characteristics.

	Patients (n = 72)
Female	20
Male	52
Age (Mean ± Std)	70.1 ± 11.3
Time since stroke (hour)	7.23 ± 9.90
NIHSS on admission (Mean ± Std)	8.47 ± 6.57
Classification label (cases)	⩽4.5 h (42); >4.5 h (30)

2.2. Methods

The methods in this study can be divided into five parts (seen in Figure 2): (1) Image Processing; (2) Infarct Lesions and Whole Brain Segmentation; (3) Feature Extraction; (4) Feature Selection and Combination Strategy; (5) Performance Evaluation.
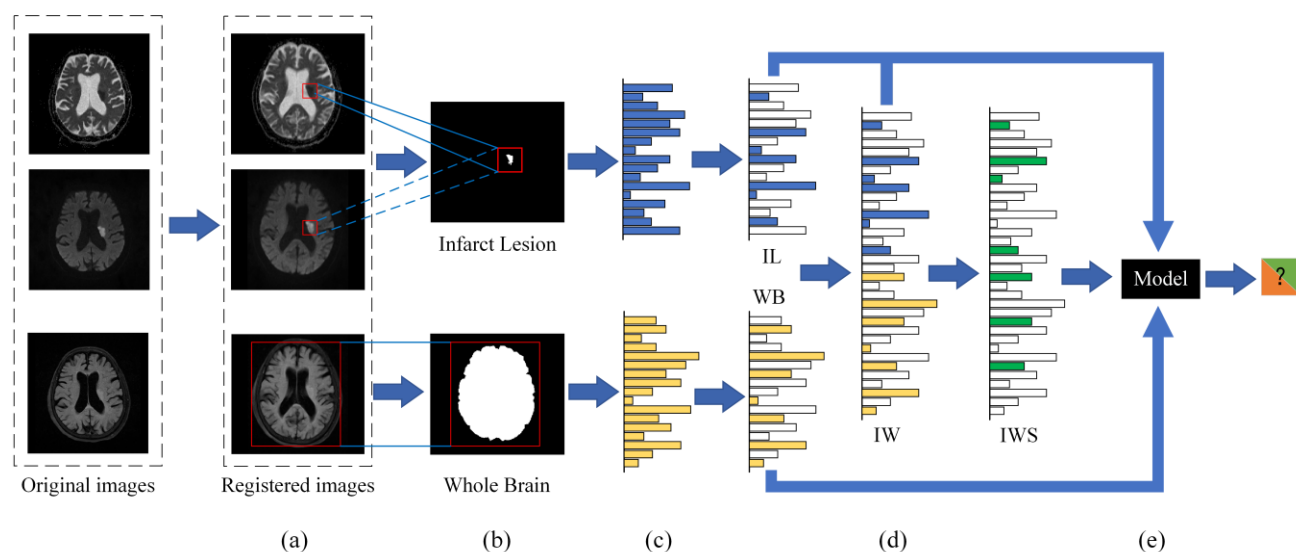

Figure 2. The whole process of methods: (a) Image processing; (b) Infarct lesions and whole brain segmentation; (c) Feature extraction; (d) Feature selection and combination strategy; (e) Performance evaluation.

2.2.1.   Image Processing

The main focus of image processing is image registration to reduce the impact of positional deviation

between images on the experimentation and to prepare for the segmentation of infarct lesions and the whole brain. The original FLAIR sequences were registered at Montreal Neurological Institute (MNI) space through a 12-degree-of-freedom affine transformation using the neuroimaging software package FMRIB's Linear Image Registration Tool (FLIRT) [20,21]. The original DWI sequences were first registered onto original FLAIR sequences and then registered onto MNI space to obtain registered images and corresponding transformation matrices. Then, original DWI sequences were registered onto MNI space according to conversion matrices.

2.2.2.   Infarct lesions and whole brain segmentation

In this study, we employed the normalization threshold method proposed by Lee et al. [22] to automatically segment the infarct lesions. The method consists of two major components: Initial segmentation and false-positive removal. After skull stripping, the initial segmentation begins by constructing a percentile intensity curve for the ADC sequences. The x-axis represents percentiles, and the y-axis represents the intensity of the ADC sequences. Subsequently, tangents are drawn at this curve's maximum and minimum derivative points. The intensity value at the intersection of these two tangents is considered the peak intensity of the ADC intensity histogram. Each voxel's intensity in the ADC sequence is then divided by this peak intensity to obtain the adjusted ADC sequence. This adjusted ADC sequence is subjected to initial segmentation using a threshold of 0.835. The initial segmentation results are mapped onto DWI sequences in the second step. The average intensity (μ_{global}) and standard deviation (SD_{global}) of the DWI sequence within this region are calculated. Then, a fine segmentation threshold is computed using the formula $T = \mu_{global} + 1.5 * SD_{global}$. Regions with intensities lower than this threshold are defined as false positives and are removed to obtain the final infarct segmentation results.

The whole brain mask was produced using the Brain Extraction Tool (BET) [23,24], which performed brain extraction operations on the registered FLAIR sequence, generated by the brain tissue mask and skull mask. Then, the brain tissue mask can be regarded as the whole brain mask in FLAIR, ADC and DWI sequences.

2.2.3.   Radiomics features extraction

We extracted radiomics features from the registered DWI, ADC and FLAIR sequences of infarct lesions and whole brain. Including six original feature groups: First-order statistics (First_order), gray-level co-occurrence matrix (GLCM), gray-level run-length matrix (GLRLM), gray-level size-zone matrix (GLSZM), gray-level dependency matrix (GLDM) and neighboring gray-tone difference matrix (NGTDM). Then, six filters were used to process the original feature groups, including log sigma with scale {1.0,2.0,3.0,4.0,5.0}, wavelet, square, square root, logarithm and exponential [25,26]. We also summarized the filtering results into the original feature groups to categorize the features. The calculated features were renamed by connecting their original name, sequence type and extraction region. The radiomics features extraction from the images was automatically performed using the PyRadiomics software package in Python 3.9 [28]. For each sequence, 1674 radiomics features were extracted for both infarct lesions and whole brain, respectively, including 324 first-order features, 432 GLCM features, 288 GLRLM features, 288 GLSZM features, 90 NGTDM features and 252 GLDM features.

2.2.4. Radiomics features selection and combination strategy

In this study, we combined the *t*-tests algorithm, least absolute shrinkage and selection operator (Lasso) to select the extracted features. This was done to explore the impact of different combinations of radiomic features to determine the onset time of AIS. Before feature selection, in order to eliminate the influence of the difference of dimensionality and value between features, and to speed up the calculation of feature dimension reduction, Equation (1) was used in this study to normalize the feature vectors.

$$F_i^* = (F_i - \overline{F_i})/(F_{imax} - F_{imin}) \tag{1}$$

where F_i^* is the normalized result of the feature F_i, the variables $\overline{F_i}$, F_{imax} and F_{imin} are the mean, maximum and minimum of F_i, respectively; and the i is the order of features.

Then, the normalized features were subjected to a t-test algorithm, and the significant radiomics features with values of $p < 0.05$ remained. After that, the retained features were selected using the Lasso algorithm, and effective features related to the target variable remained. As an effective feature selection method for choosing target-variable-related features, Lasso has found applications in various domains [29]. We implemented Lasso feature selection using the LassoCV function from scikit-learn (LassoCV (alpha = alphas, cv = 10, max_iter = 100,000, normalize = False)) in Python 3.9. Here, alphas represent the regularization weight, and in our research, we employed a range of alpha values (alpha = np.logspace(−10, 1, 500, base=2)) to determine the features. To better compare the research outcomes, four experimental groups were established based on different feature combination strategies: IL, WB, IW and IWS. IL was infarct lesion features that were obtained by performing the above feature screening operation, WB was the whole brain features that were obtained by the same operation, IW was the direct combination of IL and WB features and IWS was the features result after another Lasso feature selection of IW features.

2.2.5. Performance evaluation

The obtained radiomic features were provided as input into ten different classification models, and we used ten-fold cross-validation to calculate the models' parameters to evaluate the prediction model's performance. In order to ensure an equal representation of positive and negative samples in both the training and test sets, we implemented the StratifiedKFold(n_splits = K) function, where K = 10, indicating the division of the dataset into ten subsets. All classification models were implemented in Python 3.9, including nine machine learning models: Support vector machine (SVM) with "sklearn.svm.SVC(kernel = 'rbf', probability = True)", multilayer perceptual neural network (NN) with "sklearn.neural_network. MLPClassifier(hidden_layer_sizes = (400, 100), alpha = 0.01, max_iter = 10,000)", random forest (RF) with "sklearn.ensemble.RandomForestClassifier(n_estimators = 200)", decision tree (DT) with "sklearn.tree.DecisionTreeClassifier()", k-nearest neighbors (KNN) with "sklearn.neighbors. sklearn.neighbors()", Adaboost classifier (Ada) with "sklearn.ensemble.AdaBoostClassifier()", logistic regression (LR) with "sklearn.linear_model.logisticRegressionCV(max_iter = 100,000, solver = "liblinear")", GaussianNB (NB) with "sklearn.naive_bayes.GaussianNB()", gradient boosting classifier (GBDT) with "sklearn.ensemble.GradientBoostingClassifier()" and one statistical classification model: linear discriminant analysis (DA) with "sklearn.discriminant_analysis.LinearDiscriminantAnalysis()".

3. Results

3.1. Selected radiomics features

After feature selection and combination, 39 features were selected for the IL group, 42 for the WB group and 31 for the IWS group (seen in Figure 3(a)). Furthermore, we labeled 81 features selected separately from infarct lesions and the whole brain as F1 to F81. Upon observation, it was found that only two features, "logarithm_glcm_Correlation_adc" and "wavelet-LHH_firstorder_Mean_flair" appeared in both the IL and WB groups (seen in Figure 3(b)).
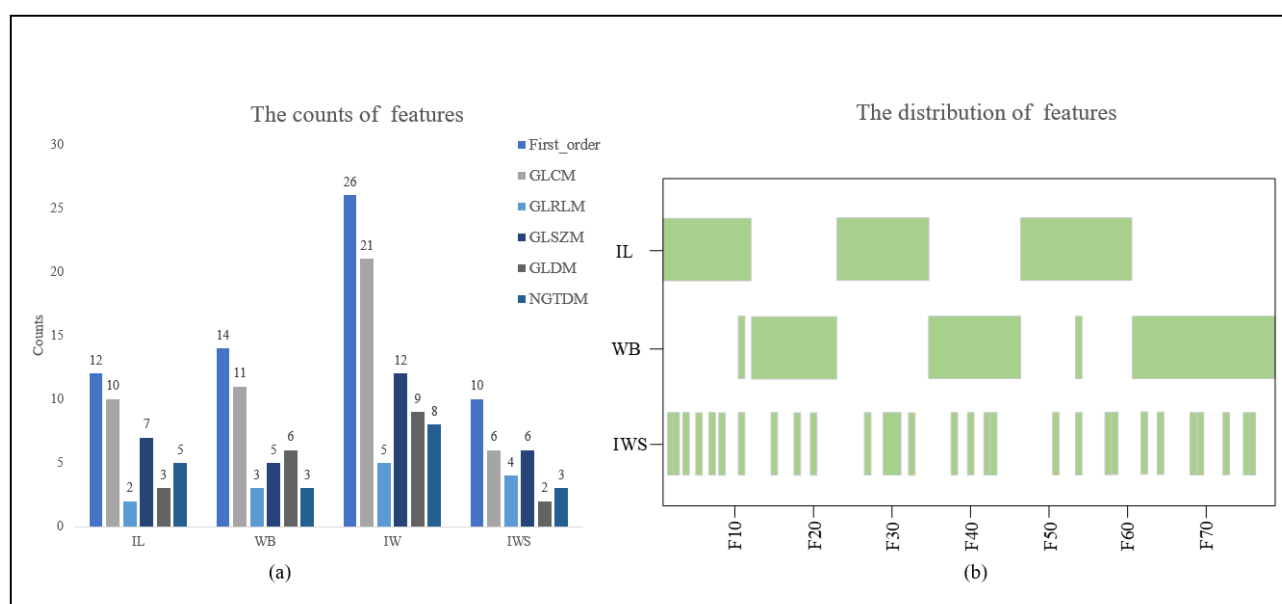

Figure 3. The counts and distribution of features in four experimental groups: (a) Counts of the selected features in IL, WB, IW and IWS; (b) the distribution of the selected features, F1–F79 are the features series.

3.2. Performance of four experimental groups

In this study, we assessed the classification performance of all experimental groups (IL, WB, IW, IWS) to determine AIS onset time by analyzing the performance parameters of multiple classification models. These performance parameters included AUC, accuracy (acc), precision (pre), F1 score (F1) and recall. We primarily focused on presenting and explaining the AUC, with the remaining parameters displayed only for the recommended models. Table 2 shows the AUCs of the four experimental groups using features from ADC, DWI and FLAIR sequences across ten classification models. The range of AUCs for IL, WB, IW and IWS were as follows: 0.699 ± 0.089, 0.640 ± 0.045, 0.754 ± 0.080, 0.795 ± 0.096. The SVM and RF models achieved the best AUC of 0.769 in the IL group. WB group achieved the best AUC of 0.717 (NN), lower than IL's. Moreover, for the same models, the AUCs of the WB group were generally lower than those of the IL group, with only NN and DA models showing some improvement. Regardless of whether considering the best AUC or the AUC for individual models, the IW group outperformed the IL and WB groups. The IW group's best AUC was 0.862 (SVM),

significantly higher than the IL group (0.769) and the WB group (0.717). Only the AUC for RF, Ada and GBDT models showed slight decreases compared to the IL group. The IWS group performed the best among the four experimental groups, achieving the best AUC of 0.904 (NN) and the AUCs of each model were also generally the highest among all experimental groups, and compared to the IW group, only DT and Ada exhibited decreased AUCs.

Table 2. The AUCs of four experimental groups with the ADC_DWI_FLAIR sequence combination.

Classifier	IL	WB	IW	IWS
SVM	0.769	0.644	0.862	0.887
NN	0.707	0.717	0.837	0.904
RF	0.769	0.632	0.746	0.787
DT	0.631	0.618	0.652	0.632
KNN	0.721	0.638	0.767	0.854
Ada	0.729	0.570	0.721	0.704
LR	0.757	0.692	0.829	0.867
NB	0.752	0.654	0.804	0.871
GBDT	0.677	0.580	0.636	0.688
DA	0.478	0.657	0.682	0.757
Mean ± Std	0.699 ± 0.089	0.640 ± 0.045	0.754 ± 0.080	0.795 ± 0.096

The results in Table 2 indicate that the performance parameters of the IWS group's models are generally superior to those of the IL, WB and IW groups. This feature combination is also proposed and recommended in this study. Therefore, we will continue to present the remaining parameters of the IWS group models with the ADC_DWI_FLAIR sequence combination, as shown in Table 3, to validate the accuracy and effectiveness of this method. Similar to the AUC values, the performance metrics for SVM and NN models surpass those of the other models, with the NN model performing the best. Specifically, the NN model achieves acc, pre, F1 and recall values of 0.916, 0.939, 0.904 and 0.909, respectively.

Table 3. The performance parameters of the IWS group with the ADC_DWI_FLAIR sequence combination.

Classifier	ACC	PRE	F1	RECALL
SVM	0.904	0.931	0.887	0.894
NN	0.916	0.939	0.904	0.909
RF	0.803	0.813	0.787	0.789
DT	0.646	0.622	0.632	0.619
KNN	0.873	0.913	0.854	0.858
Ada	0.718	0.725	0.704	0.699
LR	0.873	0.888	0.867	0.867
NB	0.873	0.901	0.871	0.864
GBDT	0.707	0.695	0.688	0.675
DA	0.761	0.802	0.757	0.744
Mean ± Std	0.807±0.094	0.823±0.111	0.795±0.096	0.792±0.102

To better explore the relationships and patterns between the experimental groups, we also conducted controlled experiments using different combinations of sequences, including the use of a single sequence ("ADC", "DWI", "FLAIR"), as well as a combination of two sequences ("ADC_DWI", "ADC_FLAIR", "DWI_FLAIR"). Table 4 shows the AUCs of the two best models SVM and NN from previous results, and the best AUCs in each experimental group. In the "DWI_FLAIR" sequence combination, the best AUC of IWS, and the AUCs of SVM and NN, are significantly higher than those of the IL, WB and IW groups. Similarly, in the "ADC_FLAIR" and "ADC_DWI" sequence combinations, IWS exhibited the best AUC, with both SVM and NN outperforming the other three groups. In the "FLAIR" sequence combination, only the AUC (0.708) of NN in IWS is lower than IW (0.723), while the rest are the highest AUCs in the IWS group. In the "DWI" sequence combination, the IWS group had the highest AUC. In the "ADC" sequence combination, only the AUC (0.728) of NN in IWS is lower than IL (0.734), while the rest are the highest in the IWS experimental group.

Table 4. The AUCs of four experimental groups with the additional sequence combinations.

Sequence combination	Classifier	IL	WB	IW	IWS
DWI_FLAIR	Best	0.817	0.730	0.808	0.871
	SVM	0.804	0.659	0.792	0.825
	NN	0.728	0.717	0.808	0.837
	Mean ± Std	0.742 ± 0.070	0.654 ± 0.063	0.748 ± 0.057	0.781 ± 0.078
ADC_FLAIR	Best	0.732	0.711	0.790	0.871
	SVM	0.723	0.711	0.771	0.854
	NN	0.665	0.636	0.748	0.871
	Mean ± Std	0.674 ± 0.061	0.615 ± 0.081	0.703 ± 0.094	0.781 ± 0.080
ADC_DWI	Best	0.807	0.717	0.850	0.896
	SVM	0.753	0.628	0.798	0.879
	NN	0.790	0.653	0.724	0.811
	Mean ± Std	0.738 ± 0.055	0.632 ± 0.060	0.746 ± 0.071	0.784 ± 0.091
FLAIR	Best	0.717	0.677	0.742	0.762
	SVM	0.683	0.561	0.700	0.712
	NN	0.634	0.614	0.723	0.708
	Mean ± Std	0.633 ± 0.066	0.578 ± 0.063	0.644 ± 0.080	0.684 ± 0.065
DWI	Best	0.812	0.703	0.827	0.836
	SVM	0.740	0.630	0.761	0.797
	NN	0.709	0.556	0.751	0.801
	Mean ± Std	0.741 ± 0.041	0.606 ± 0.067	0.748 ± 0.044	0.770 ± 0.042
ADC	Best	0.734	0.718	0.788	0.817
	SVM	0.667	0.707	0.758	0.817
	NN	0.734	0.590	0.726	0.728
	Mean ± Std	0.681 ± 0.044	0.612 ± 0.096	0.716 ± 0.062	0.745 ± 0.083

4. Discussion

Accurately determining the onset time in AIS patients holds significant clinical importance for devising appropriate treatment protocols, predicting patient prognosis and facilitating recovery outcomes. Currently, there are two major methods for determining the onset time. One is through clinical interviews, but it can be limited by the patient's condition, resulting in patients struggling to express their onset time clearly. The other method employs the DWI-FLAIR mismatch, but some studies have indicated that the accuracy of determining the onset time using image mismatch is only about 0.6 [12]. Therefore, some studies have employed patient data with precise onset time to develop ML models, and some researchers have introduced radiomics technology [16–19], demonstrating the feasibility of ML algorithms in determining stroke onset time. However, these studies often focus solely on the lesion's local features, ignoring the whole brain's global information, resulting in lower predictive accuracy of the models, failing to meet the clinical requirements. In this study, we intended to classify the onset time of AIS in patients by combining the radiomics features from both infarct lesions and whole brain of multi-sequenced MR images. It investigated the impact of different feature combinations on classification accuracy. As a result, the best AUC after combining features reached 0.904 (IWS), an improvement of 13.5% over the results using lesion features alone. This confirmed that combining infarct lesions and whole brain features could further enhance the accuracy of onset time classification.

The main cause of ischemic stroke is local brain tissue damage caused by cerebral vascular occlusion [30], manifested as local lesions on imaging. However, blood circulation occurs throughout the body. When ischemic stroke occurs, cerebral blood flow (CBF) parameters in not only the lesions but also the surrounding regions of lesions will be affected [29–31]. Some articles [32–35] have also indicated that changes in blood flow transmission in local tissues could lead to blood flow transmission and blood oxygen metabolism in surrounding tissues and even the whole brain. This means that local blockage of blood vessels may affect the tissue characteristics of the whole brain to varying degrees [36]. Therefore, we have reason to believe that the imaging findings of stroke patients are not only related to the situation of the local lesions but also to information in other regions or the whole brain, and the whole brain features may help diagnose and treat ischemic stroke. In this study, the best AUC for the experimental group using lesion features alone was 0.817 (IL, "DWI_FLAIR"), consistent with previous research results using lesion features. When using whole brain features directly to determine stroke onset time, the best AUC was 0.730 (WB, "DWI_FLAIR"). Furthermore, according to Figure 3(b), it could be observed that whole brain features were independent of lesion features. Therefore, it can be concluded that whole-brain features play a significant role in determining the onset time, and their combination may enhance the accuracy of the predictive model.

We combined lesion and whole brain features for a more comprehensive analysis. From the initial results in Table 2, it can be seen that whether combining the features directly or combining them and then selecting, the results are better than using the lesion features or whole brain features alone, with the AUCs of 0.862 (IW, "ADC_DWI_FLAIR") and 0.904 (IWS, "ADC_DWI_FLAIR"), respectively, and establishing a linear relationship as "IWS > IW > IL > WB", which not only demonstrates the potential role of whole brain features in determining the onset time of stroke but also reveals the possible relationship between infarct features and whole brain features. To validate the findings of this study, we conducted additional comparative experiments based on different combinations of sequences. The results showed that when using lesion features or whole brain features alone as models input, the

AUCs remained below 0.82. However, combining the infarct lesions and whole brain features could significantly improve the performance of the classifiers, and it can be proved that the relationship discovered in this study was not accidental and played an important role in accurately determining stroke onset time. In addition, regarding the combination of sequences, we found that the performance of classifiers using multiple sequence combinations was generally better than those using single sequences. For example, in the IWS group, the best AUC obtained from multiple sequence combinations is above 0.870. In contrast, the AUC of single sequence combinations, except for "DWI" which reaches 0.836, is significantly lower than that of multiple sequence combinations. Similarly, from the results, the IW, IL and WB groups also largely followed the above trend. Using features from multiple sequences can further enhance the accuracy of determining the onset time. We also observed that the "DWI" sequence combination seems distinct from the other two single-sequence combinations, "ADC" and "FLAIR", as its best AUC was comparable to or even higher than that of multi-sequence combinations. For instance, as shown in Table 4, in the IW group, the "DWI" sequence combination achieved the best AUC of 0.827, surpassing the best AUCs of the "DWI_FLAIR" (0.808) and "ADC_FLAIR" (0.790), and in the IWS group, the AUC for the "DWI" sequence combination reached 0.836. Therefore, in specific scenarios such as emergencies, scanning only the DWI sequence may be considered to save time and expedite patient rescue, which can be highly beneficial to the patients.

Radiomics is an image post-processing technology developed in recent years, which is widely used in the diagnosis, prognosis and prediction of diseases due to its excellent characterization ability [37–39]. Lee et al. [17] and Zhang et al. [19] have used radiomics features to determine the onset time of stroke, demonstrating the great clinical value of radiomics. The results of this study also demonstrated that using radiomics features as input to the classifier models had a good effect on determining the onset time of stroke. However, radiomics has technical limitations, including susceptibility toward image acquisition and reconstruction parameters and it is susceptible to class imbalances and image quality [40]. Therefore, the radiomics features extracted from different datasets may vary and directly impact the model performance, an inherent characteristic of radiomics [41]. This can be directly observed from Figure 3b, which shows minimal overlap in features between the IL and WB groups, indicating significant differences in radiomic features extracted from the same dataset's infarct lesion and whole brain. Moreover, MR images have their characteristics, and differences in scanning equipment, scanning methods and reconstruction algorithms can result in different output images, further affecting the extraction of features.

The patients in this study were from a single medical center, MR images were all of the exact specifications, and the sample size of patients was relatively small, which may lead to a lack of generalizability of the extracted features. This is a limitation in this study. However, it is noteworthy that the number of positive and negative samples is similar, with 42 positive and 30 negative cases, reducing the possibility of inadequate training. Thus, we performed ten-fold cross-validation to evaluate the performance of the classifier models and mitigate the impact of sample size on the evaluation results. However, there is a trade-off during feature selection. For instance, we performed it on the entire dataset (not just the 9 partitions used each time) and repeated it for each fold in the 10-fold cross-validation. This could lead to some process leakage (test set data used for feature extraction). However, considering that the impact may not be significant (using only 10% of the data), we plan to overlook and address this trade-off in future work.

Additionally, due to the limitation of the dataset size, we classified only whether the stroke onset time was within 4.5 hours. In some clinical applications, the thrombolysis time window has been

extended to 6, 9 or even 24 hours. Therefore, in future work, we will expand the dataset and validate and improve our method with more extensive and varied datasets. To further refine the classification of patient onset time, for example, we divided patients within 24 hours into one-hour intervals, and explored the patterns and relationships. Furthermore, we will consider using CT scan images for such studies and explore the possibility of identifying standardized features as inputs for the classification model, enhancing their applicability across different devices and patient populations.

5. Conclusions

In conclusion, several studies have demonstrated the feasibility of using infarct lesion features to determine the onset time of AIS. Based on the previous studies, we combined the radiomics features of multi-sequence infarct lesions and whole brain from MR images to determine AIS onset time. From the results, it can be concluded that combining lesion features with whole brain features can further improve the predictive performance. The AUC increased by 13.5% (from 0.769 to 0.904) compared to using only lesion features. Also, the selection of sequences may affect the classifier's performance, and using multiple sequences can provide more feature information to improve its classification ability. Thus, this study may provide decision guidance for clinicians in AIS treatment.

Use of AI tools declaration

We declare that no artificial intelligence (AI) tools were used at the time of writing this article.

Conflict of interest

All authors have no conflicts of interest to report.

References

1. Q. Ding, S. Liu, Y. Yao, H. Liu, T. Cai, L. Han, Global, regional, and national burden of ischemic stroke, 1990–2019, *Neurology*, **98** (2022), E279–E290. https://doi.org/10.1212/WNL.0000000000013115

2. S. Ogoh, T. Tarumi, Cerebral blood flow regulation and cognitive function: A role of arterial baroreflex function, *J. Physiol. Sci.*, **69** (2019), 813–823. https://doi.org/10.1007/s12576-019-00704-6

3. W. Hacke, M. Kaste, E. Bluhmki, M. Brozman, A. Dávalos, D. Guidetti, et al., Thrombolysis with alteplase 3 to 4.5 hours after acute ischemic stroke, *New Engl. J. Med.*, **359** (2008), 1317–1329. https://doi.org/10.1056/NEJMoa0804656

4. H. Liu, W. Hu, F. Zhang, W. Gu, J. Hong, J. Chen, et al., Efficacy and safety of rt-PA intravenous thrombolysis in patients with wake-up stroke: A meta-analysis, *Medicine*, **101** (2022), e28914. https://doi.org/10.1097%2FMD.0000000000028914

5. A. R. Al-Buhairi, M. M. Jan, Recombinant tissue plasminogen activator for acute ischemic stroke, *Neurosci. J.*, **7** (2002), 7–13.

6. A. Nelson, G. Kelly, R. Byyny, C. Dionne, C. Preslaski, K. Kaucher, Tenecteplase utility in acute ischemic stroke patients: A clinical review of current evidence, *Am. J. Emerg. Med.*, **37** (2019): 344–348. https://doi.org/10.1016/j.ajem.2018.11.018

7. B. C. Campbell, H. Ma, S. Curtze, G. A. Donnan, M. Kaste, Extending thrombolysis to 4.5–9 h and wake-up stroke using perfusion imaging: a systematic review and meta-analysis of individual patient data, *Lancet*, **394** (2019), 139–147. https://doi.org/10.1016/S0140-6736(19)31053-0

8. A. Damiza-Detmer, I. Damiza, M. Pawełczyk, Wake-up stroke-diagnosis, management and treatment, *Curr. Neurol.*, **20** (2020), 66–70. https://doi.org/10.15557/AN.2020.0009

9. A. Wouters, R. Lemmens, P. Dupont, V. Thijs, Wake-up stroke and stroke of unknown onset: a critical review, *Front. Neurol.*, **5** (2014). https://doi.org/10.3389/fneur.2014.00153

10. C. S. Anderson, T. Robinson, R. I. Lindley, H. Arima, P. M. Lavados, T. H. Lee, et al., Low-dose versus standard-dose intravenous alteplase in acute ischemic stroke, *New Engl. J. Med.*, **374** (2016), 2313–2323. https://doi.org/10.1056/NEJMoa1515510

11. J. Mackey, D. Kleindorfer, H. Sucharew, C. J. Moomaw, B. M. Kissela, K. Alwell, et al., Population-based study of wake-up strokes, *Neurology*, **76** (2011), 1662–1667. https://doi.org/10.1212/WNL.0b013e318219fb30

12. S. Emeriau, I. Serre, O. Toubas, F. Pombourcq, C. Oppenheim, L. Pierot, Can diffusion-weighted imaging-fluid-attenuated inversion recovery mismatch (positive diffusion-weighted imaging/negative fluid-attenuated inversion recovery) at 3 tesla identify patients with stroke at < 4.5 hours?, *Stroke*, **44** (2013), 1647–1651. https://doi.org/10.1161/STROKEAHA.113.001001

13. D. Buck, L. C. Shaw, C. I. Price, G. A. Ford, Reperfusion therapies for wake-up stroke: systematic review, *Stroke*, **45** (2014), 1869–1875. https://doi.org/10.1161/STROKEAHA.114.005126

14. O. M. Rønning, Reperfusion therapy in stroke cases with unknown onset, *Tidsskrift for Den norske legeforening*, **136** (2016), 1333. https://doi.org/10.4045/tidsskr.16.0626

15. Q. Chen, T. Xia, M. Zhang, N. Xia, J. Liu, Y. Yang, Radiomics in stroke neuroimaging: techniques, applications, and challenges, *Aging Dis.*, **12** (2021), 143–154. https://doi.org/10.14336%2FAD.2020.0421

16. K. C. Ho, W. Speier, H. Zhang, F. Scalzo, S. El-Saden, C. W. Arnold, A machine learning approach for classifying ischemic stroke onset time from imaging, *IEEE Trans. Med. Imaging*, **38** (2019), 1666–1676. https://doi.org/10.1109/TMI.2019.2901445

17. H. Lee, E. J. Lee, S. Ham, H. B. Lee, J. S. Lee, S. U. Kwon, et al., Machine learning approach to identify stroke within 4.5 hours, *Stroke*, **51** (2020), 860–866. https://doi.org/10.1161/STROKEAHA.119.027611

18. H. Zhu, L. Jiang, H. Zhang, L. Luo, Y. Chen, Y. Chen, An automatic machine learning approach for ischemic stroke onset time identification based on DWI and FLAIR imaging, *Neuroimage-Clin.*, **31** (2021), 102744. https://doi.org/10.1016/j.nicl.2021.102744

19. Y. Q. Zhang, A. F. Liu, F. Y. Man, Y. Y. Zhang, C. Li, Y. E. Liu, et al., MRI radiomic features-based machine learning approach to classify ischemic stroke onset time, *J. Neurol.*, **269** (2022), 350–360.

20. M. Jenkinson, S. Smith, A global optimisation method for robust affine registration of brain images, Med. Image Anal., **5** (2001), 143–156. https://doi.org/10.1016/S1361-8415(01)00036-6

21. M. M. Jenkinson, P. Bannister, M. Brady, S. Smith, Improved optimisation for the robust and accurate linear registration and motion correction of brain images, *Neuroimage*, **17** (2002), 825–841. https://doi.org/10.1006/nimg.2002.1132

22. H. Lee, K. Jung, D. W. Kang, N. Kim, Fully automated and real-time volumetric measurement of infarct core and penumbra in diffusion-and perfusion-weighted MRI of patients with hyper-acute stroke, *J. Digit. Imaging*, **33** (2020), 262–272. https://doi.org/10.1007/s10278-019-00222-2

23. S. M. Smith, Fast robust automated brain extraction, *Hum. Brain Mapp.*, **17** (2002), 143–155. https://doi.org/10.1002/hbm.10062

24. M. Jenkinson, M. Pechaud, S. Smith, BET2: MR-based estimation of brain, skull and scalp surfaces, in *Eleventh Annual Meeting of the Organization for Human Brain Mapping*, **17** (2005), 167.

25. J. J. M. Van Griethuysen, A. Fedorov, C. Parmar, A. Hosny, N. Aucoin, V. Narayan, et al., Computational radiomics system to decode the radiographic phenotype, *Cancer Res.*, **77** (2017), e104–e107. https://doi.org/10.1158/0008-5472.CAN-17-0339

26. Y. Zhang, B. Zhang, F. Liang, S. Liang, Y. Zhang, P. Yan, et al., Radiomics features on non-contrast-enhanced CT scan can precisely classify AVM-related hematomas from other spontaneous intraparenchymal hematoma types, *Eur. Radiol.*, **29** (2019), 2157–2165. https://doi.org/10.1007/s00330-018-5747-x

27. Muthukrishnan, R. and R. Rohini. LASSO: A feature selection technique in predictive modeling for machine learning, in *2016 IEEE International Conference on Advances in Computer Applications (ICACA)*, (2016), 18–20. https://doi.org/10.1109/ICACA.2016.7887916

28. X. Wu, H. Wang, F. Chen, L. Jin, J. Li, Y. Feng, et al., Rat model of reperfused partial liver infarction: characterization with multiparametric magnetic resonance imaging, microangiography, and histomorphology, *Acta Radiol.*, **50** (2009), 276–287. https://doi.org/10.1080/02841850802647021

29. C. Wang, P. Miao, J. Liu, Z. Li, Y. Wei, Y. Wang, et al., Validation of cerebral blood flow connectivity as imaging prognostic biomarker on subcortical stroke, *J. Neurochem.*, **159** (2021), 172–184. https://doi.org/10.1111/jnc.15359

30. D. A. Hernandez, R. P. H. Bokkers, R. V. Mirasol, M. Luby, E. C. Henning, J. G. Merino, et al., Pseudocontinuous arterial spin labeling quantifies relative cerebral blood flow in acute stroke, *Stroke*, **43** (2012), 753–758. https://doi.org/10.1161/STROKEAHA.111.635979

31. C. Wang, P. Miao, J. Liu, S. Wei, Y. Guo, Z. Li, et al., Cerebral blood flow features in chronic subcortical stroke: Lesion location-dependent study, *Brain Res.*, **1706** (2019), 177–183. https://doi.org/10.1016/j.brainres.2018.11.009

32. T. Love, D. Swinney, E. Wong, R. Buxton, Perfusion imaging and stroke: A more sensitive measure of the brain bases of cognitive deficits, *Aphasiology*, **16** (2002), 873–883. https://doi.org/10.1080/02687030244000356

33. M. H. Lev, A. Z. Segal, J. Farkas, S. T. Hossain, C. Putman, G. J. Hunter, et al., Utility of perfusion-weighted CT imaging in acute middle cerebral artery stroke treated with intra-arterial thrombolysis-Prediction of final infarct volume and clinical outcome, *Stroke*, **32** (2001), 2021–2027. https://doi.org/10.1161/hs0901.095680

34. C. Grefkes, G. R. Fink, Connectivity-based approaches in stroke and recovery of function, *Lancet Neurol.*, **13** (2014), 206–216. https://doi.org/10.1016/S1474-4422(13)70264-3

35. M Giacalone, P Rasti, N Debs, C Frindel, TH Cho, E. Grenier, Local spatio-temporal encoding of raw perfusion MRI for the prediction of final lesion in stroke, *Med. Image Anal.*, **50** (2018), 117–126. https://doi.org/10.1016/j.media.2018.08.008

36. J. D. Jordan, W. J. Powers, Cerebral autoregulation and acute ischemic stroke, *Am. J. Hypertens.*, **25** (2012), 946–950. https://doi.org/10.1038/ajh.2012.53

37. X. Yao, L. Mao, S. Lv, Z. Ren, W. Li, K. Ren, CT radiomics features as a diagnostic tool for classifying basal ganglia infarction onset time, *J. Neurol. Sci.*, **412** (2020), 116730. https://doi.org/10.1016/j.jns.2020.116730

38. Z. Yi, L. Long, Y. Zeng, Z. Liu, Current advances and challenges in radiomics of brain tumors, *Front. Oncol.*, **11** (2021). https://doi.org/10.3389/fonc.2021.732196

39. Y. Zhang, B. Zhang, F. Liang, S. Liang, Y. Zhang, P. Yan, et al., Radiomics features on non-contrast-enhanced CT scan can precisely classify AVM-related hematomas from other spontaneous intraparenchymal hematoma types, *Eur. Radiol.*, **29** (2019), 2157–2165. https://doi.org/10.1007/s00330-018-5747-x

40. M. E. Mayerhoefer, A. Materka, G. Langs, I. Häggström, P. Szczypiński, P. Gibbs, et al., Introduction to radiomics, *J. Nucl. Med.*, **61** (2020), 488–495. https://doi.org/10.2967/jnumed.118.222893

41. M. Zhou, J. Scott, B. Chaudhury, L. Hall, D. Goldgof, K. W. Yeom, et al., Radiomics in brain tumor: Image assessment, quantitative feature descriptors, and machine-learning approaches, *Am. J. Neuroradiol.*, **39** (2018), 208–216.